PHYSICAL REVIEW B **92**, 140405(R) (2015)

Domain wall magneto-Seebeck effect

Patryk Krzysteczko,* Xiukun Hu, Niklas Liebing, Sibylle Sievers, and Hans W. Schumacher
Physikalisch-Technische Bundesanstalt, Bundesallee 100, D-38116 Braunschweig, Germany
(Received 14 April 2015; published 6 October 2015)

The interplay between charge, spin, and heat currents in magnetic nanostructures subjected to a temperature gradient has led to a variety of novel effects and promising applications studied in the fast-growing field of spin caloritronics. Here, we explore the magnetothermoelectrical properties of an individual magnetic domain wall in a permalloy nanowire. In thermal gradients of the order of few K/μm along the long wire axis, we find a clear magneto-Seebeck signature due to the presence of a single domain wall. The observed domain wall magneto-Seebeck effect can be explained by the magnetization-dependent Seebeck coefficient of permalloy in combination with the local spin configuration of the domain wall.

DOI: 10.1103/PhysRevB.92.140405 PACS number(s): 75.75.−c, 72.15.Jf

Electronic transport coefficients in ferromagnetic materials are spin dependent, enabling important spintronics applications [1]. This observation also holds for magnetothermoelectrical (or spin caloritronic) phenomena [2–4] driven by thermal gradients [5–8]. In a thermal gradient, the temperature difference ΔT between two contacts gives rise to a thermopower $V_T = -S\Delta T$, with S being the material's Seebeck coefficient. Spin-dependent Seebeck coefficients have been observed in various nanomagnetic systems such as thin films [9,10], multilayers [11], tunnel junctions [12–14], and nanowires [15–17]. In the latter, magnetization reversal often occurs by the nucleation and propagation of a single magnetic domain wall (DW), enabling promising applications such as DW logic circuits [18] or spin-transfer torque driven DW memories [19].

The high current densities applied in such devices also induce strong thermal gradients which in turn can interact with the DW [20–25], with prospects for thermally driven DW motion [26,27] or nanoscale magnetic heat engines [28]. The local spin structure of the DW itself should further lead to a DW magneto-Seebeck signal which might in turn enable new device functionalities. However, these fundamental thermoelectrical properties of a single magnetic DW have not been investigated yet. In this Rapid Communication we study this missing link between nanomagnetism and thermoelectricity by exploring the magneto-Seebeck characteristics of a magnetic DW in a permalloy nanowire. We find a clear DW magneto-Seebeck signal which is consistent with the the magnetization-dependent Seebeck coefficient of permalloy and the local spin configuration of the DW.

In our experiments we use L-shaped permalloy (Py) nanowires with a notch [see Fig. 1(a) and the Supplemental Material [29] for details]. The L's corner allows a controlled nucleation of a DW while the notch stops a moving DW between the electrical probes. The two probes contact the Py wire from the top for resistance and thermopower measurements. Two additional Pt strips located at a distance of 0.5 and 1.5 μm from the Py nanowire serve as the resistive thermometer and heater, respectively. The magnetic behavior of the system is characterized by two-wire resistance measurements as a function of magnetic field at a dc current of 600 μA. In a first step, the magnetization of the entire wire is rotated from the longitudinal ($\parallel$) to the transversal ($\perp$) direction by a magnetic field applied at $\phi = 90^\circ$, i.e., along the y direction [note the definition of coordinates in Fig. 1(a)].

As expected for a system dominated by anisotropic magnetoresistance (AMR), the measurement shows a bell-shaped curve [Fig. 2(a)] with resistance being decreased by the field of either polarity by $\Delta R = R_\parallel - R_\perp$. We find $R_\parallel = 289.8\ \Omega$ at remanence and $R_\perp = 288.5\ \Omega$ at maximum transversal field and hence a two-wire AMR ratio $\Delta R/R_\perp = 0.45\%$. In a second step, we study the AMR contribution of a single DW. For this purpose we apply a 120 mT field in the diagonal direction ($\phi_{set} = -135^\circ$) to create a head-to-head DW at the corner which is moved towards the notch by a field applied at any $|\phi| < 80^\circ$. As an example, Fig. 2(b) shows a measurement at $\phi = 0^\circ$. The DW arrives at the notch at H_1, where it remains until H_2 is reached. The presence of the DW at the notch leads to a decrease of resistance by approximately 0.17 Ω. The resistance drop is due to transversally oriented magnetization within the DW and based entirely on AMR. The critical fields H_1 and H_2 are the pinning fields of the corner and of the notch, respectively. To fully characterize the DW dynamics we repeat the measurement in the angle range $|\phi| < 80^\circ$. The results are presented in Fig. 1(c), where the resistance is indicated by a color scale. The yellow region indicates the resistance lowered due to the presence of the DW at the notch. Typically, the left edge of this region is smooth whereas the right edge is rather irregular. This shows that the pinning strength of the corner $H_1(\phi)$ for various angles is well defined [30] while the pinning strength of the notch $H_2(\phi)$ has a stronger stochastic component. We model the magnetization distribution during field-driven DW motion by micromagnetic simulations using a Landau-Lifshitz-Gilbert micromagnetic simulator [29]. Our numerical analysis predicts that a vortex type of DW is nucleated at the corner as pictured in Fig. 3(d), where the magnetization distribution at $\mu_0 H = 20$ mT during a field sweep at $\phi = -30^\circ$ is shown. For increasing field strength, the vortex DW will be "pulled" deeper into the notch, deformed, and finally transformed into a transversal DW before depinning, which explains the stochastic behavior of $H_2(\phi)$.

For thermoelectrical measurements, we generate temperature gradients by applying an ac power P at a frequency of $f = 262$ Hz to the heater. To characterize the temperature distribution, we use calibration samples with identical heaters

*patryk.krzysteczko@ptb.de

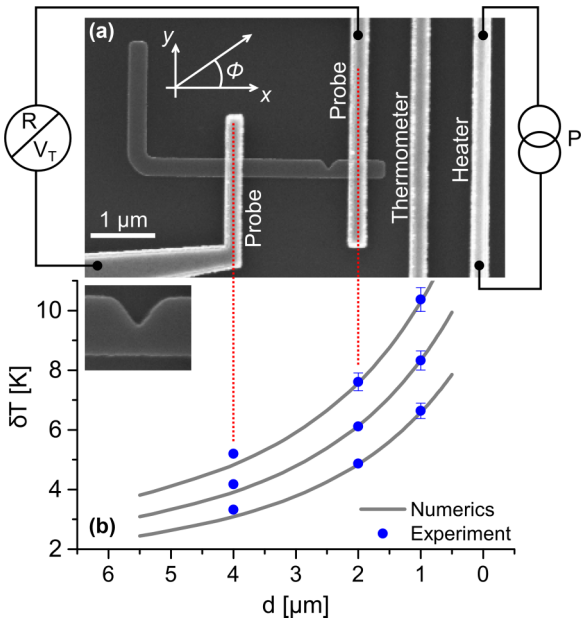

FIG. 1. (Color online) Sample geometry and temperature distribution. (a) Micrograph of the L-shaped permalloy nanostructure with Pt contact probes for voltage and resistance measurements. The inset below shows the notch with higher magnification. The coordinate system and the direction of the external magnetic field are indicated by the white arrows. (b) The temperature increase for three heater powers $P = 17$, 22, and 27 mW as a function of the distance to the heater. Experimental results are shown by blue bullets; numerical results (gray lines) show a good agreement.

and thermometers placed correspondingly to the positions of the voltage probes [red lines in Fig. 1(a)]. For each heater power P, the thermometer resistance has a $2f$ ac component with amplitude $\delta R(P)$ detected by four-wire lock-in measurements (see Ref. [29] for more details). To translate δR to the temperature increase δT, we first determine the temperature coefficient α_{Pt} in a separate setup. We find $\alpha_{\mathrm{Pt}} = 0.0013\ \mathrm{K}^{-1}$, which is 30% of the bulk value, in good agreement with literature [31]. Figure 1(b) shows the measured δT (blue bullets) as a function of the distance d from the heater for three heating powers: 17, 22, and 27 mW. The temperature distribution is further investigated by three-dimensional finite-element modeling [29]. The numerical results (gray lines) show a good agreement with the experimental data. Heating with 27 mW leads to an increase of the nanowire temperature of up to 10 K and a ΔT between the probes of (2.4 ± 0.5) K. In the following, the thermopower V_{T} is measured at $P = 27$ mW by lock-in detection at $2f$ via the voltage probes.

Figure 2(d) shows the evolution of the thermopower V_{T} as a function of transversal field [$\phi = 90^\circ$, cf. Fig. 2(a)]. Again, a bell-shaped curve comes into view, but with the thermopower being *increased* by a magnetic field of either polarity. We find a thermopower of $V_{\mathrm{T}\parallel} = 56.08\ \mu$V at remanence and $V_{\mathrm{T}\perp} = 56.54\ \mu$V at maximum field with an accuracy of ± 10 nV. The effective Seebeck coefficient is $S = (23 \pm 6)\ \mu$V/K. The magnetothermopower (MTP) ratio $(V_{\mathrm{T}\parallel} - V_{\mathrm{T}\perp})/V_{\mathrm{T}\perp}$ yields $(-0.81 \pm 0.03)\%$. The Seebeck coefficient of the nanowire thus rises when the wire's magnetization rotates under the action of an external field. For a comparison of the magnetoresistance (MR) and magneto-Seebeck ratio, the lead contributions have to be taken into account, as discussed in the Supplemental Material [29]. In the following, we investigate the change of thermopower induced by the presence of a single DW. As an example, Fig. 2(e) shows a MTP measurement at the same conditions as the MR measurement shown in Fig. 2(b). As the field reaches $\mu_0 H = 4$ mT, we observe a sudden increase of thermopower by approximately 40 nV. The thermopower remains roughly constant at this level until the field reaches 21 mT, where it drops back to the base level. Figure 2(f) shows the complete set of DW thermopower (DWTP) measurements for angles $|\phi| < 80^\circ$. In this color plot, the yellow area indicates the increased thermopower. If we compare the pinning fields from MR and thermopower measurements [Figs. 2(c) and 2(f)], and keep the stochastic nature of H_2 in mind, we can safely consider them as identical. Evidently, the origin of increased thermopower is the same as the origin of reduced resistance, namely, the presence of a DW at the notch. The data thus clearly reveal the thermoelectrical signature of a single DW.

To analyze our data, we describe the thermopower of a system magnetized along the x direction by

$$\nabla V_{\mathrm{T}} = -\begin{pmatrix} S_\parallel & 0 & 0 \\ 0 & S_\perp & -S_N \\ 0 & S_N & S_\perp \end{pmatrix} \nabla T, \tag{1}$$

where the Seebeck coefficient has a tensor character analogous to the resistivity tensor (see the Supplemental Material [29]). The diagonal elements of the tensor represent the anisotropy of the Seebeck coefficient; $S_\parallel$ is measured when the temperature gradient is parallel to the magnetization direction while $S_\perp$ is measured when it is transversal to the magnetization direction [cf. Fig. 2(d)]. We consider also the anomalous Nernst effect (ANE) by the off-diagonal elements $S_N = -2.6\ \mu$V/K, which will generate an additional thermopower in the case of a nonvanishing out-of-plane temperature gradient [32]. Our experimental setup is designed to detect the thermopower generated along the wire direction, thus we consider only the x component of Eq. (1). The resulting MTP can be described by three terms,

$$\begin{aligned} V_{\mathrm{T}} = &-[S_\perp + \Delta S \cos^2(\theta)]\Delta T_x \\ &- \Delta S \cos(\theta)\sin(\theta)\Delta T_y \\ &- S_N \sin(\theta)\Delta T_z, \end{aligned} \tag{2}$$

where θ is the angle of the local magnetization direction with respect to the x direction [29]. Due to the analogy with AMR, we refer to the first term as the anisotropic magneto-Seebeck (AMS) effect. The second term is related to the planar Nernst effect (PNE) [9], and the third term describes the ANE contribution of an in-plane magnetized system. We use numerical results of magnetization distribution and temperature gradients to verify this approach. The nanowire is divided in cells of $10 \times 10\ \mathrm{nm}^2$. For each cell we take the local magnetization direction $\theta(x, y)$ and the temperature difference across the cell to calculate the local thermopower according to Eq. (2). To estimate the global thermopower, we calculate the mean thermopower generated in each 10-nm section of the wire and integrate between the voltage probes. We repeat those

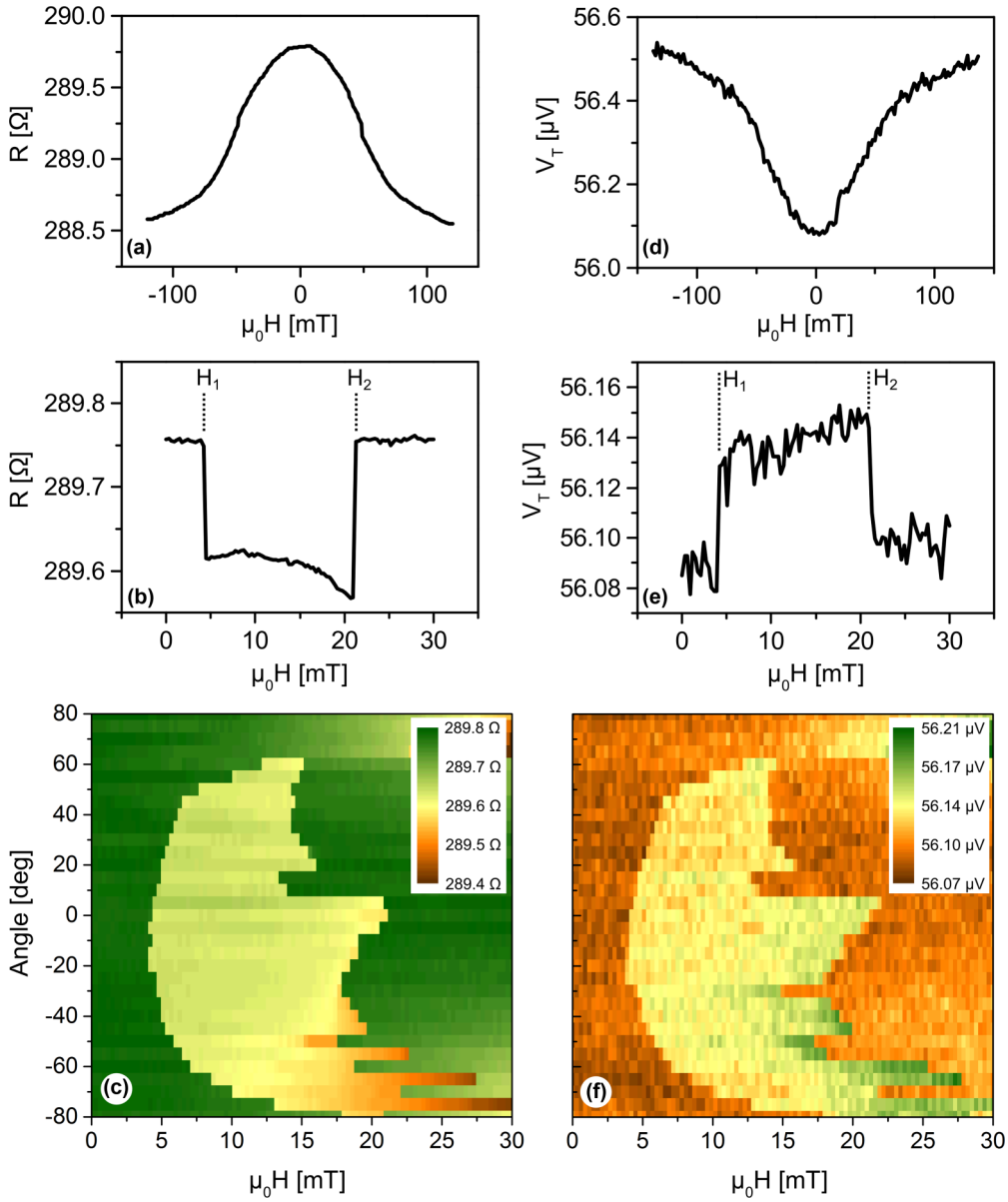

FIG. 2. (Color online) Magnetoresistance and magnetothermopower measurement. (a) The resistance R of the wire vs applied field $\mu_0 H$ measured in transversal geometry ($\phi = 90°$). (b) Domain wall magnetoresistance measured at $\phi = 0°$. The pinning fields of the corner and the notch are indicated by H_1 and H_2, respectively. (c) A set of domain wall magnetoresistance measurements for angles $|\phi| < 80°$. The resistance is indicated by the color scale. (d) The thermopower of the wire measured in transversal geometry ($\phi = 90°$). (e) Domain wall magnetothermopower measured at $\phi = 0°$. (f) A set of domain wall magnetothermopower measurements for all angles $|\phi| < 80°$. The thermopower is indicated by the color scale.

calculations for various magnetic configurations [one example is shown in Fig. 3(d)] corresponding to the movement of a DW during a field sweep at $\phi = -30°$. The temperature gradients are pictured as color maps in Figs. 3(e)–3(g) (note the different color scales for in-plane and out-of-plane directions).

Figure 3(a) shows the measured DWTP for $\phi = -30°$ with the thermopower of the remanent state $V_{T\|}$ set to zero. The calculation considering only the AMS is shown in Fig. 3(b) by the blue curve. Taking the typical deviations of a micromagnetic model into account, a very good agreement between experiment and simulation is obtained. Our analysis thus reveals that the DWTP is dominated by the AMS [the first term in Eq. (2)] and the remaining terms of Eq. (2) are treated as corrections. The expected PNE contribution is indicated by the green line in Fig. 3(c). It shows a nearly constant value of approximately 15 nV with a DW signature of only 3 nV. Within the experimental noise level, PNE should hence have no impact on the DWTP. Figure 3(c) also plots the ANE contribution (brown line). The curve starts at roughly 15 nV with a gradual increase and a DW signature of 7 nV. However, at 30 mT the ANE signal shows a sudden drop and a change of sign. Here, the magnetization direction at the hot side of the notch is reversed due to the depinning of the DW. In the remaining upsweep to 60 mT and the downsweep to 0 mT again a linear behavior is found. The ANE should thus lead to a splitting of the signal at zero field, as shown by the gray

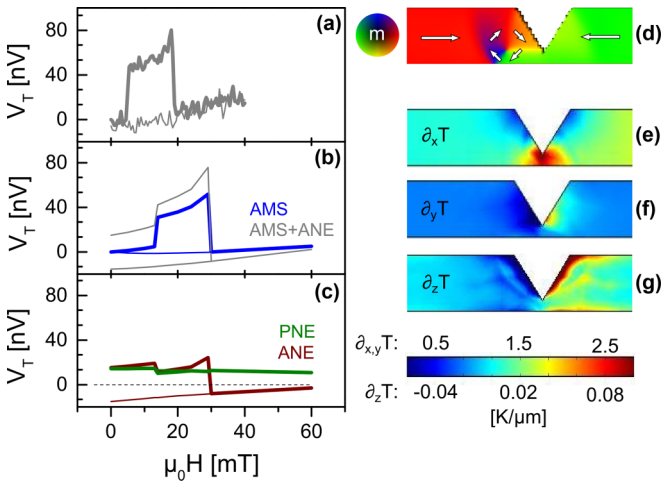

FIG. 3. (Color online) (a) Domain wall magnetothermopower measured at $\phi = -30^\circ$ (upsweep, thick line; downsweep, thin line). The graph shows the thermopower change with respect to the remanent state $V_{T\|}$. (b) The calculated AMS contribution (blue) and the calculated contribution due to AMS and ANE acting together (gray). (c) Calculated contribution due to PNE (green) and ANE (brown). (d) Example of a simulated magnetization distribution showing a vortex DW. The local magnetization direction is indicated by the color scale. (e)–(g) The calculated temperature gradient in the x, y, and z directions.

curve in Fig. 3(b). Clearly, this splitting is not observed in the experiment. From that we can conclude that the ANE is not significant in the experimental data and seems to be overestimated by the model. Note that the temperature model is based on a wire with sharp rectangular cross sections and a sharp V-shaped notch. This leads to an overestimation of the out-of-plane gradients at the notch and hence of the ANE contribution compared to the real device with rounded edges and smooth notch (cf. Fig. 1 inset).

Similar results have been obtained on various devices with varying geometries, confirming that a slight variation of the nanowire width or the notch shape does not change the general behavior. Furthermore, no significant difference between head-to-head and tail-to-tail DWs was found. Our data thus clearly reveal the thermopower contribution of an individual DW in a magnetic nanowire, thereby providing the fundamental link between the macroscopic thermoelectrical signature and the nanoscopic spin configuration. These findings open the path for future fundamental studies of DW thermoelectricity. For example, in narrow DWs, an intrinsic DWTP contribution resulting from spin mistracking inside the DW should be present analogous to the intrinsic DW magnetoresistance [33–36]. Furthermore, new DW devices and functionalities are possible, such as the recently proposed DW thermocouple [37] or the thermoelectric DW detection.

This work has been developed under the EMRP JRP IND 04 SpinCal, jointly funded by EU and EMRP participating countries within EURAMET. We thank Deutsche Forschungsgemeinschaft for financial support through SPP 1538. Support in sample fabrication by T. Weimann is highly acknowledged. The Py film was grown at the Center for Spinelectronic Materials and Devices in Bielefeld by M. Glas.

[1] I. Žutić, J. Fabian, and S. D. Sarma, Rev. Mod. Phys. **76**, 323 (2004).
[2] M. Johnson and R. H. Silsbee, Phys. Rev. B **35**, 4959 (1987).
[3] G. E. W. Bauer, A. H. MacDonald, and S. Maekawa, Solid State Commun. **150**, 459 (2010).
[4] G. E. W. Bauer, E. Saitoh, and B. J. van Wees, Nat. Mater. **11**, 391 (2012).
[5] K. Uchida, Nature (London) **455**, 778 (2008).
[6] A. Slachter, F. L. Bakker, J. P. Adam, and B. J. van Wees, Nat. Phys. **6**, 879 (2010).
[7] J.-C. LeBreton, S. Sharma, H. Saito, S. Yuasa, and R. Jansen, Nature (London) **475**, 82 (2011).
[8] K.-R. Jeon, B.-C. Min, A. Spiesser, H. Saito, S.-C. Shin, S. Yuasa, and R. Jansen, Nat. Mater. **13**, 360 (2014).
[9] A. D. Avery, M. R. Pufall, and B. L. Zink, Phys. Rev. Lett. **109**, 196602 (2012).
[10] M. Schmid, S. Srichandan, D. Meier, T. Kuschel, J.-M. Schmalhorst, M. Vogel, G. Reiss, C. Strunk, and C. H. Back, Phys. Rev. Lett. **111**, 187201 (2013).
[11] J. Shi, R. C. Yu, S. S. P. Parkin, and M. B. Salamon, J. Appl. Phys. **73**, 5524 (1993).
[12] M. Czerner, M. Bachmann, and C. Heiliger, Phys. Rev. B **83**, 132405 (2011).
[13] M. Walter, J. Walowski, V. Zbarsky, M. Muenzenberg, M. Schaefers, D. Ebke, G. Reiss, A. Thomas, P. Peretzki, M. Seibt *et al.*, Nat. Mater. **10**, 742 (2011).
[14] N. Liebing, S. Serrano-Guisan, K. Rott, G. Reiss, J. Langer, B. Ocker, and H. W. Schumacher, Phys. Rev. Lett. **107**, 177201 (2011).
[15] L. Gravier, S. Serrano-Guisan, F. Reuse, and J. P. Ansermet, Phys. Rev. B **73**, 024419 (2006).
[16] T. Böhnert, V. Vega, A.-K. Michel, V. M. Prida, and K. Nielsch, Appl. Phys. Lett. **103**, 092407 (2013).
[17] T. Böhnert, A. C. Niemann, A.-K. Michel, S. Bäßler, J. Gooth, B. G. Tóth, K. Neuróhr, L. Péter, I. Bakonyi, V. Vega *et al.*, Phys. Rev. B **90**, 165416 (2014).
[18] D. A. Allwood, G. Xiong, C. C. Faulkner, D. Atkinson, D. Petit, and R. P. Cowburn, Science **309**, 1688 (2005).
[19] S. S. P. Parkin, M. Hayashi, and L. Thomas, Science **320**, 190 (2008).
[20] L. Berger, J. Appl. Phys. **58**, 450 (1985).
[21] M. Hatami, G. E. W. Bauer, Q. Zhang, and P. J. Kelly, Phys. Rev. Lett. **99**, 066603 (2007).
[22] A. A. Kovalev and Y. Tserkovnyak, Phys. Rev. B **80**, 100408 (2009).
[23] D. Hinzke and U. Nowak, Phys. Rev. Lett. **107**, 027205 (2011).
[24] F. Schlickeiser, U. Ritzmann, D. Hinzke, and U. Nowak, Phys. Rev. Lett. **113**, 097201 (2014).
[25] J. Chico, C. Etz, L. Bergqvist, O. Eriksson, J. Fransson, A. Delin, and A. Bergman, Phys. Rev. B **90**, 014434 (2014).

[26] J. Torrejon, G. Malinowski, M. Pelloux, R. Weil, A. Thiaville, J. Curiale, D. Lacour, F. Montaigne, and M. Hehn, Phys. Rev. Lett. **109**, 106601 (2012).

[27] W. Jiang, P. Upadhyaya, Y. Fan, J. Zhao, M. Wang, L.-T. Chang, M. Lang, K. L. Wong, M. Lewis, Y.-T. Lin *et al.*, Phys. Rev. Lett. **110**, 177202 (2013).

[28] G. E. W. Bauer, S. Bretzel, A. Brataas, and Y. Tserkovnyak, Phys. Rev. B **81**, 024427 (2010).

[29] See Supplemental Material at http://link.aps.org/supplemental/10.1103/PhysRevB.92.140405 for details on device fabrication, temperature calibration, the influence of the wiring, micromagnetic simulations, temperature distribution modeling, and the derivation of the Seebeck tensor.

[30] H. Corte-Leon, V. Nabaei, A. Manzin, J. Fletcher, P. Krzysteczko, H. W. Schumacher, and O. Kazakova, Sci. Rep. **4**, 6045 (2014).

[31] X. Zhang, H. Xie, M. Fujii, H. Ago, K. Takahashi, T. Ikuta, H. Abe, and T. Shimizu, Appl. Phys. Lett. **86**, 171912 (2005).

[32] A. Slachter, F. L. Bakker, and B. J. van Wees, Phys. Rev. B **84**, 020412 (2011).

[33] P. M. Levy and S. Zhang, Phys. Rev. Lett. **79**, 5110 (1997).

[34] G. Tatara and H. Fukuyama, Phys. Rev. Lett. **78**, 3773 (1997).

[35] R. P. van Gorkom, A. Brataas, and G. E. W. Bauer, Phys. Rev. Lett. **83**, 4401 (1999).

[36] C. Hassel, M. Brands, F. Y. Lo, A. D. Wieck, and G. Dumpich, Phys. Rev. Lett. **97**, 226805 (2006).

[37] P. Krzysteczko and H. Schumacher, DE Patent No. 102,014,201,415 (19 March 2015).